# Hybrid Lead Halide Iodide and Lead Halide Bromide in Efficient Hole Conductor Free Perovskite Solar Cell

Sigalit Aharon, Bat El Cohen, and Lioz Etgar*

Institute of Chemistry, Casali Center for Applied Chemistry, The Hebrew University of Jerusalem, Edmond J. Safra Campus, Givat Ram, Jerusalem 91904, Israel

Ⓢ Supporting Information

ABSTRACT: In this work we used $CH_3NH_3PbI_nBr_{3-n}$ (where $0 \leq n \leq 3$) as hole conductor and light harvester in the solar cell. Various concentrations of methylammonium iodide and methylammonium bromide were studied which reveal that any composition of the hybrid $CH_3NH_3PbI_nBr_{3-n}$ can conduct holes. The hybrid perovskite was deposited in two steps, separating it to two precursors to allow better control of the perovskite composition and efficient tuning of its band gap. The X-ray diffraction reveals the change in the lattice parameter due to the introducing of the Br^- ions. The hybrid iodide/bromide perovskite hole conductor free solar cells show very good stability, their power conversion efficiency achieved 8.54% under 1 sun illumination with current density of 16.2 mA/cm². The results of this work open the possibility for graded structure of perovskite solar cells without the need for hole conductor.
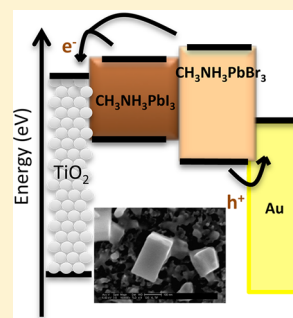
INTRODUCTION

Solar cells are a key technology for sustainable energy supply. A photovoltaic device is based on the photoelectric effect, which requires the charge separation of electrons and holes in a light absorbing material to conductive contacts that transmit electricity.

Recently, a breakthrough occurs in the field by using organic−inorganic perovskite as light harvester in solar cells. The structure of the organic−inorganic perovskite is AMX_3, where M is a divalent cation, X are halides, and A is the organic part, generally a cation consisting of a monolayer or a bilayer. Organic−inorganic perovskite has optimal properties enabling use as a light harvester in a solar cell, including direct band gap, large absorption coefficients,[1] and high carrier mobility,.[2,3] Today the power conversion efficiency (PCE) of perovskite-based solar cells is reaching over 16% using different deposition techniques.[4−6] A long-range electron−hole diffusion length was found in organometallic perovskite absorber, justifying the high efficiency achieved for perovskite-based solar cells.[7,8] Moreover the hole transport properties of these organic−inorganic perovskites was demonstrated by using them as light harvester and as hole conductor simultaneously.[9] Initially these cells deliver PCE of 5%, which was improved recently to 8[10] and 10.8%.[11,12] Avoiding the use of hole transport material in these high efficiency solar cells has several advantages, for example, lower cost, long-term stability, and the simple structure of the solar cell.

One of the important properties of the organic−inorganic perovskite for their use in photovolatic cells is the possibility to tune their optical properties (e.g., band gap). This can be achieved by changing the halide anions surrounding the metal cation. This possibility of tuning the optical properties was supported by theoretical modeling, which found good agree-ment between the calculated band structures and the experimental trend of optical band gaps in these perovskites structures.[13]

As a consequence of the possibility to tune the band gap, high-voltage solar cells were demonstrated with open circuit voltage (V_{oc}) of 1.15 and 1.3 V using $CH_3NH_3PBr_3$ as sensitizer and poly[N-9-hepta-decanyl-2,7-carbazole-*alt*-3,6-bis(thiophen-5-yl)-2,5-dioctyl-2,5-dihydropyrrolo[3,4-]pyrrole-1,4-dione] (PCBTDPP) or N,N′-dialkylperylenediimide (PDI) as hole transport materials[14,15]

Seok et al. showed colorful, efficient perovskite solar cells using different Br concentrations in the perovskite achieving PCE of 12.3% using polytriarylamine (PTAA) as the hole conductor. In their work, the common one-step deposition technique was used, when the two precursors of the perovskite were mixed together and deposited on the substrate in one step by spin coating.[16]

In this work, we combine two important properties of the perovskite, its capability to conduct holes in particular for hybrid perovskites that contain bromide, and the possibility to tune the perovskite band gap. Hybrid $CH_3NH_3PbI_nBr_{3-n}$ (where $0 \leq n \leq 3$) perovskites was sensitized and deposited onto mesoporous TiO_2 using a two-step deposition technique, which allows better control of the hybrid perovskite composition and its corresponding band gap. X-ray diffraction (XRD) reveals the change in the lattice parameter due to the introducing of the Br^- ions. Hole conductor free solar cells using the hybrid $CH_3NH_3PbI_nBr_{3-n}$ were developed that prove

the possibility of the $CH_3NH_3PbI_nBr_{3-n}$ to conduct holes in addition to its functionality as a light harvester. We demonstrate power conversion efficiency of 8.54% under 1 sun illumination with current density of 16.2 mA/cm^2 for these hybrid lead halide iodide/bromide perovskite solar cells without a hole conductor.

■ RESULTS AND DISCUSSION

Figure 1A shows the structure of the hole conductor free solar cell. The solar cell consists of conductive glass and thin TiO$_2$
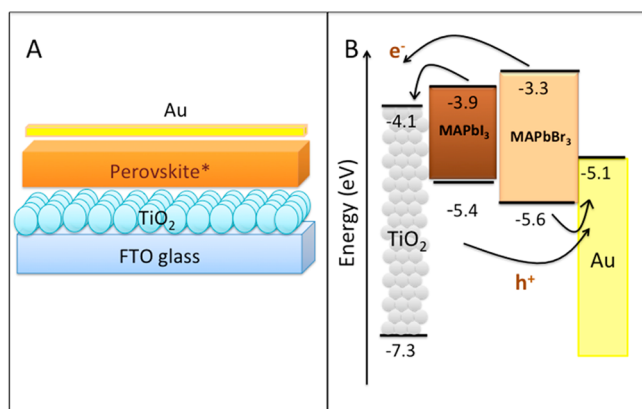

Figure 1. (A) Structure of the hybrid lead halide iodide and lead halide bromide hole conductor free perovskite solar cell. The perovskite* indicates that the perovskite structure consists of different MAI and MABr (CH_3NH_3=MA) concentrations investigated in this study. (B) Energy level diagram of the pure MAPbI$_3$ and the pure MAPbBr$_3$ perovskites used in this work. The positions of the energy levels are according to ref 13.

nanoparticles film; on top of the TiO$_2$ film, a perovskite layer is deposited (can be observed in Figure 2B as an over layer on top
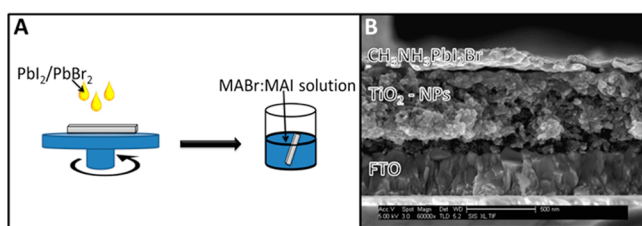

Figure 2. Schematic illustration of the two-step deposition technique of the mixed halide perovskite film. MA corresponds to $CH_3NH_3^+$. (B) HR-SEM cross section of one of the solar cells discussed in this work. The $CH_3NH_3PbI_2Br$ perovskite can be seen as an over layer on the TiO$_2$ film.

the TiO$_2$ film) that consists of perovskite composition according to the formula $CH_3NH_3PbI_nBr_{3-n}$ (where $0 \leq n \leq 3$). No hole conductor is used in these solar cells that result in

hole conductivity through the hybrid $CH_3NH_3PbI_nBr_{3-n}$. This is the first report demonstrating hole transport in perovskite containing Br. The back contact of the device is a thin film of evaporated gold. The energy level diagram is presented in Figure 1B; both pure $CH_3NH_3PbI_3$ and $CH_3NH_3PbBr_3$ can inject electrons to the TiO$_2$ and transfer the holes to the gold back contact; as a result, the energy level position of the hybrid structure $CH_3NH_3PbI_nBr_{3-n}$ would be suitable for the operation of the cell (discussed in further detail below).

Description of the deposition of the perovskite film by two-step technique is the following: the PbI$_2$ or PbBr$_2$ is spin coated on the TiO$_2$ film resulting in a thin uniform layer of PbI$_2$/PbBr$_2$ on the TiO$_2$ surface. The annealed PbI$_2$ or PbBr$_2$ layer is dipped into a mixed solution of MAI and MABr (CH_3NH_3= MA); different concentrations in the dipping solution are studied (see Table 1). During the dipping process, the MAI and the MABr react with the PbI$_2$ or the PbBr$_2$ creating the perovskite crystals. Using the two-step deposition technique, more control over the perovskite composition is achieved, in contrast to the one-step deposition technique (spin coating the entire solution of the components together). Devices using the spin technique with different Br- and I- contractions were fabricated as well (see Supporting Information).

Figure 2 presents schematic illustration of the two-step deposition of the hybrid halide perovskite film. Representative high-resolution scanning electron microscopy (HR-SEM) image of the hybrid hole conductor free solar cell ($CH_3NH_3PbI_2Br$) is shown in Figure 2B, the perovskite film can be seen as an over layer on top of the TiO$_2$, therefore it is capable of transporting electrons and holes. The thickness of the TiO$_2$ film was 500 ± 50 nm (measured by profiler) and the perovskite film was 150 ± 50 nm thick. Possibly some of the perovskite was penetrated inside the pores; this results with an efficient electron transfer between the perovskite and the TiO$_2$.[17] On the other hand, we can assume that the recombination occurred in these cells is mainly between electrons in the TiO$_2$ and holes in the perovskite, therefore we expect that less recombination will occur when the pores are not completely filled. In this work, high V_{oc} of around 0.8 V and high FF of 68% were achieved indicating that the pores probably are not completely filled with perovskite. (These are relatively high values when discussing on the situation where no hole conductor is being used.) Moreover, it is also important to note that efficient planar perovksite solar cells were reported where no mesoporous film was required for the operation of the cell.[7]

When comparing two different dipping times in the cation solution (MAI or MABr), a change in the morphology of the crystals can be observed (Figure 3). In the case of the PbI$_2$+MAI ($CH_3NH_3PbI_3$), no difference is observed between 2 s of dipping and 30 s of dipping. However, when looking on different dipping times in the case of PbI$_2$+MABr, after 2 s of dipping there are still areas where there are not any perovskite

Table 1. Photovoltaic Parameters of the Solar Cells and Their Energy Band Gap

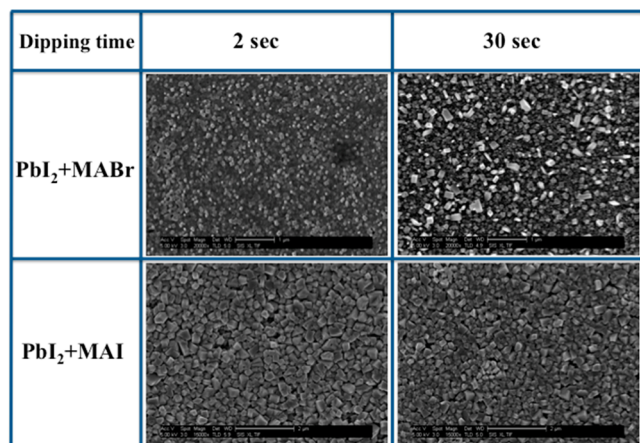| spin solution	MABr/MAI Molar ratio in Dip solution	V_{oc} (V)	J_{sc} (mA/cm^2)	FF	efficiency (%)	E_g (eV)	R_s (ohm)
PbI$_2$	0:1 ($CH_3NH_3PbI_3$)	0.77	15.6	60	7.2	1.51	65.6
PbI$_2$	1:2	0.77	16.2	68	8.54	1.58	61.7
PbI$_2$	2:1	0.71	13.5	58	5.64	1.65	76.7
PbI$_2$	1:0	0.75	9.6	35	2.55	1.72	185.5
PbBr$_2$	1:0 ($CH_3NH_3PbBr_3$)	0.79	4.7	46	1.69	2.12	350.3

Figure 3. HR-SEM figures of PbI₂+MABr and PbI₂+MAI samples at different dipping time in the MABr or MAI solution, respectively.

crystals while after 30 s of dipping most the crystals are formed. This suggests that the cation interacts differently depends on its halide.

Changing the halogen is affecting the optical properties of the perovskite. Figure 4 presents the absorption spectra of the
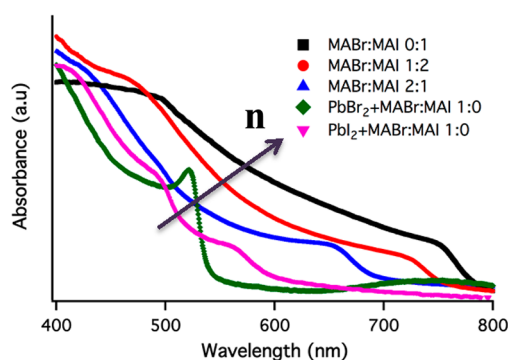

Figure 4. Absorption spectra of the different perovskites composition. The arrow indicates the increase in n.

various perovskite compositions, the PbBr₂+MABr/MAI 1:0 indicates the CH₃NH₃PbBr₃ perovskite with a band gap of 2.12 eV, while the PbI₂+MABr/MAI 0:1 indicates the CH₃NH₃PbI₃ perovskite with a band gap of 1.51 eV. The other samples show different concentrations of MAI and MABr in the dipping

solution corresponding to various band gaps. The range of the band gaps, which are calculated according to tauc plots (see Figure S2 in the Supporting Information), is between 1.51 to 2.12 eV, suitable for the hole conductor free solar cells because the conduction band position is higher than the TiO₂ conduction band, and the valence band position is lower than the gold work function.

As described above, the exciton absorption bands shifted to short wavelength (higher photon energy) when introducing the Br ions. The position of the absorption peak is determined by the Br(4p) orbitals with the Pb(6s) orbitals (related to the valence band of the CH₃NH₃PbI$_n$Br$_{3-n}$ perovskite). The transitions in the methylammonium lead halide perovskite are similar to the transitions in PbI₂.[18,19] The valence band of the PbI₂ was composed of Pb(6s) orbitals and I(5p) orbitals while the conduction band was composed of Pb(6p) orbitals. Moreover, the energy level of Br(4p) is lower than the energy level of Pb(6s), therefore the peak position of CH₃NH₃PbI$_n$Br$_{3-n}$ is influenced and shifted to higher energy.[20]

The XRD spectra are shown in Figure 5A. The diffraction peaks of the various cells are observed, showing the crystallographic structure of the samples. In all cells where Br⁻ ions are involved, the diffraction peaks correspond to the cubic structure, although in the case of CH₃NH₃PbI₃ (where there are no Br⁻ ions), the peaks are related to the tetragonal structure. Figure 5B shows a magnification of the XRD spectra in the range of $27° \leq 2\theta \leq 31°$.

The position of the (002) diffraction peak for the samples is changed according to the Br⁻ concentrations. In the case of the CH₃NH₃PbI₃, two peaks can be observed, indexed as (220) and (004) related to the tetragonal structure. These two diffraction peaks are merged into one when introducing the Br into the perovskite structure. As a result of the implementation of the Br⁻ ions into the perovskite structure, the lattice parameter changes from 5.921 for the CH₃NH₃PbBr₃, 6.144 for the MABr/MAI 2:1, and 6.223 for the MABr/MAI 1:2. The change in the lattice parameter is due to the difference in the ionic radius of Br⁻ (1.96A) and I⁻ (2.2A).[12] The smaller ionic radius of the Br⁻ is the main reason for the formation of the cubic structure when Br is introduced into the perovskite structure.

The difference in the shape of the perovskite crystals due to Br substitutions can be also observed in the HR-SEM top view figures (Figure 6). Figure 6A,B show perovskite films with the composition of CH₃NH₃PbBr₃ and CH₃NH₃PbI₃, respectively.
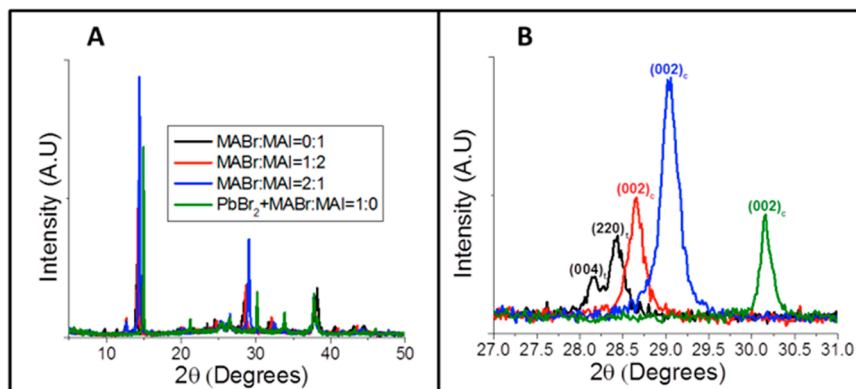

Figure 5. (A) XRD diffraction of the different samples contains different Br⁻ ions concentrations. (B) XRD spectra in the range of $27° \leq 2\theta \leq 31°$. The Miller indexes are mentioned on the figure. "c" corresponds to cubic and "t" corresponds to tetragonal.
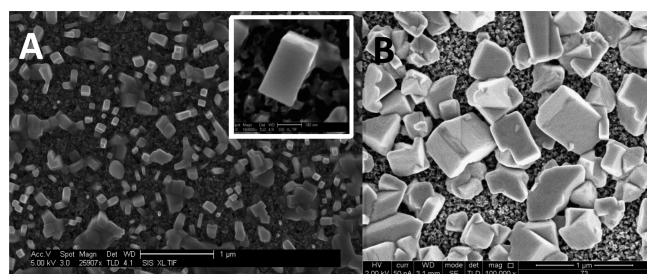
Figure 6. HR-SEM top view of $CH_3NH_3PbBr_3$ (A) and $CH_3NH_3PbI_3$ (B). (Inset) Single $CH_3NH_3PbBr_3$ crystal. The scale bar is 100 nm.

In the case of the $CH_3NH_3PbBr_3$ (Figure 6A), the shapes are more cubic than in Figure 6B of the $CH_3NH_3PbI_3$.

The photovoltaic results of the hybrid perovskite hole conductor free solar cells are summarized in Table 1. An important, novel observation from these results is the possibility of the various perovskites containing Br to conduct holes (since no hole transport material is used in these cells). The pure $CH_3NH_3PbI_3$ achieved power conversion efficiency (PCE) of 7.2% at a light illumination of 100 mW cm^{-2} AM 1.5G. On the other hand, the $CH_3NH_3PbBr_3$ achieved the lowest PCE of 1.69%. PCE of 8.54% was achieved with the molar ratio of MABr to MAI (in the dip solution) as 1:2.

A possible reason for this PCE could be due to the suitable band gap determined by the iodide, while the partial substitution of the bromide could provide (as discussed later) better stability and has smaller effect on the photovoltaic performance; finally, the combination of both achieved higher PCE than the $CH_3NH_3PbI_3$.

Figure 7A presents the $J-V$ curves of these cells. When increasing the Br concentration in the perovskite composition the J_{sc} is reduced that is related to the blue shift in the absorption spectra. On the other hand, we expected that the V_{oc} would be increased because of the widening of the band gap as a result of increasing the Br concentration, however just slightly

higher V_{oc} was observed in the perovskites containing high Br concentrations. The fact that no hole transport material is being used influences the behavior of the V_{oc}; in addition, the charge transport and recombination behavior of the $CH_3NH_3PbI_nBr_{3-n}$ when acting as light harvester and hole conductor might be different in the range of $2 > n > 0.5$. As a result, the best PCEs were observed at $3 \geq n \geq 2$.

The series resistance (R_s) influences the efficiency of the solar cell. In Table 1 and Figure 7C, the R_s values for the various concentrations are presented. The efficiencies observed for the cells are in good agreement with the R_s values, which indicates that the lowest R_s values are related to the best PCE observed both for MABr/MAI 1:2 and for $CH_3NH_3PbI_3$ hole conductor free cells.

The incident photons to current efficiency (IPCE) spectra are shown in Figure 7B. The shape of the IPCE spectra is in good agreement with the absorption spectra. All cells achieved their high IPCE in the range of 400−550 nm wavelengths. The drop in the IPCE spectra at longer wavelengths corresponds to its absorption spectra; moreover, when no hole conductor is being used, the charge carriers at the back contact (gold contact) are not efficiently extracted which is attributed to the carrier collection at longer wavelengths (explains the decrease in the IPCE spectra from 550 nm wavelength). The integration of the IPCE spectra gives 3.5 mA/cm^2 for the $CH_3NH_3PbBr_3$, 9.7 mA/cm^2 for the PbI_2+MABr/MAI 1:0, 13.7 mA/cm^2 for the PbI_2+MABr/MAI 2:1, 16.55 mA/cm^2 for the PbI_2+MABr/MAI 1:2, and 15.6 mA/cm^2 for the $CH_3NH_3PbI_3$, which is in very good agreement with the J_{sc} observed by the solar simulator. The stability of the cells is shown in Figure 7D, and the efficiency was normalized related to the efficiency of the best cell. The cells were unencapsulated and measured under ambient conditions. The $CH_3NH_3PbI_3$ and the PbI_2+MABr/ MAI 1:2 cells show good stability after 80 days without affecting their efficiency. However, for the $CH_3NH_3PbBr_3$ the efficiency dropped almost to zero after few days. The hybrid
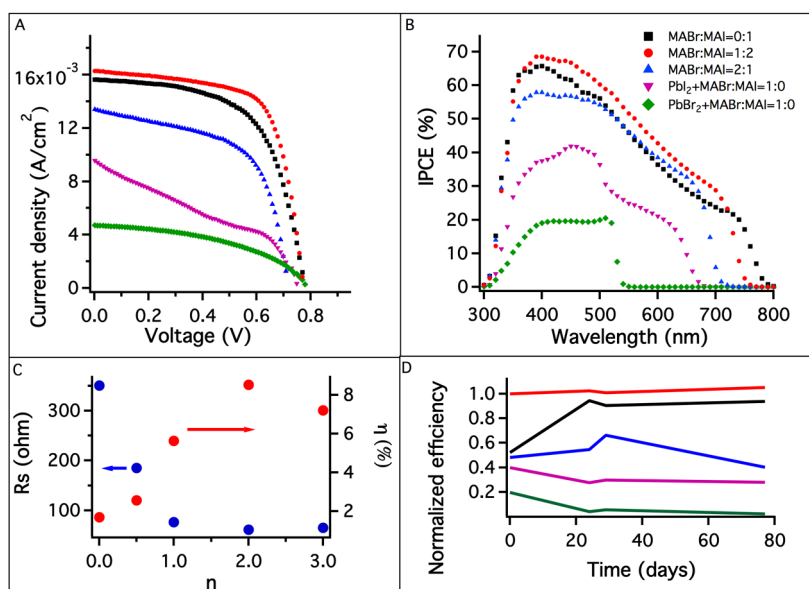

Figure 7. (A) Current−voltage curves of the different hole conductor free perovskite solar cells and their (B) corresponding IPCE spectra. (C) The PCE and the R_s values as a function of the different Br and I concentrations. n indicates the perovskite composition according to the formula $CH_3NH_3PbI_nBr_{3-n}$ (where $0 \leq n \leq 3$). (D) Stability of the different hybrid perovskite hole conductor free cells. The normalized efficiency is according to the efficiency of the best cell.

cells show good stability for this time period, which suggests of the high stability of the cubic perovskite structure as described earlier.[16]

CONCLUSION

An efficient hybrid lead halide bromide/iodide perovskite hole conductor free solar cell was presented. Avoiding the use of hole transport material in these high-efficiency solar cells has several advantages, for example: lower cost, long-term stability, and the simple structure of the solar cell. The hybrid perovskite was deposited by a two-step deposition technique permitting control of the perovskite composition and its band gap. Reflectance measurements using integrating sphere provide the absorption coefficient of the hybrid structures that assist in calculating the band gaps. XRD measurements show the change in the lattice parameter due to introducing the Br^- ions. The best hybrid $CH_3NH_3PbI_nBr_{3-n}$ perovskite hole conductor free solar cell achieved PCE of 8.54% with improved stability compared to $CH_3NH_3PbI_3$ without Br substitution.

EXPERIMENTAL SECTION

Method and Device Fabrication. CH_3NH_3I and CH_3NH_3Br were synthesized as described earlier[12,21] by reacting 30 mL of methylamine (40% in methanol, TCI) and 32.3 mL of hydroiodic acid (57 wt % in water, Aldrich) or 23.32 mL of hydrobromic acid (48 wt % in water, Aldrich) in a 250 mL round-bottom flask at 0 °C for 2h with stirring. The precipitate was recovered by putting the solution on a rotavap and carefully removing the solvents at 50 °C. The yellowish raw product of methylammonium iodide (CH_3NH_3I) or methyl-ammonium bromide (CH_3NH_3Br) was washed with ethanol by stirring the mixture for 30 min. Then the mixture was filtered and washed with diethyl ether. The washing step was repeated three times. After filtration, the solid was collected and dried at 60 °C in a vacuum oven for 24 h.

Device Fabrication. The substrate of the device was a SNO_2/F (FTO) conducting glass (15 Ω cm^{-1}, Pilkington). A blocking layer was deposited on the FTO glass using a solution of titanium diisopropoxide bis(acetylacetonate) (TiDIP, 75% in isopropanol, Aldrich) in ethanol. The TiDIP solution was spin coated and then annealed at 450 °C for 35 min. The TiO_2 solution was spin coated and annealed at 500 °C for 30 min subsequent to $TiCl_4$ treatment for 30 min at 70 °C and annealing at 500 °C for 30 min.

The synthesis of the $CH_3NH_3PbI_nBr_{3-n}$ on the TiO_2 surface was carried out by a two-step deposition technique.

At the beginning, PbI_2 or $PbBr_2$ was dissolved in DMF and dropped onto the TiO_2 film and spin coated followed by annealing at 70 °C for 30 min. In the second step, the cell was dipped into the dipping solution where different MAI to MABr molar ratios were used in isopropanol. The various molar ratio are MABr/MAI 1:0, MABr/MAI 2:1, MABr/MAI 1:2, and MABr/MAI 0:1. Following the dipping step the samples were annealed at 70 °C for another 30 min.

During the dip and the annealing, the $CH_3NH_3PbI_nBr_{3-n}$ was formed, indicated by the dark brown color of the electrode. Finally, the back contact was deposited by evaporating 50 nm of gold under pressure of 5×10^{-6} Torr. The active area was 0.09 cm^2.

X-ray Diffraction. X-ray powder diffraction measurements were performed in grazing incidence X-ray diffraction (GIXRD) mode on the D8 Advance diffractometer (Bruker AXS, Karlsruhe, Germany) with a goniometer radius of 217.5 mm, a secondary graphite monochromator, 2° Soller slits and a 0.2 mm receiving slit. XRD patterns within the range 5° to 60° 2θ were recorded at room temperature using CuKa radiation (l 1/4 1.5418°A) with the following measurement conditions: tube voltage of 40 kV, tube current of 40 mA, step-scan mode with a step size of 0.02° 2θ and counting time of 1−3 s per step. The value of the grazing incidence angle was 2.5°.

Photovoltaic Characterization. Photovoltaic measurements were made on a New Port system, composed of Oriel I−V test station using an Oriel Sol3A simulator. The solar simulator is class AAA for spectral performance, uniformity of irradiance, and temporal stability. The solar simulator is equipped with a 450 W xenon lamp. The output power is adjusted to match AM1.5 global sunlight (100 mW cm^{-2}). The spectral match classifications are IEC60904-9 2007, JIC C 8912, and ASTM E927−05. I−V curves were obtained by applying an external bias to the cell and measuring the generated photocurrent with a Keithley model 2400 digital source meter. The voltage step and delay time of photocurrent were 10 mV and 40 ms, respectively. Oriel IQE-200 was used to determine the monochromatic incident photon-to-electric current conversion efficiency. Under full computer control, light from a 150 W xenon arc lamp was focused through a monochromator in the 300−1800 nm wavelength range onto the photovoltaic cell under test. The monochromator was incremented through the visible spectrum to generate the IPCE (λ) as defined by IPCE (λ) = 12 400 ($J_{sc}/\lambda\varphi$), where λ is the wavelength, J_{sc} is the short-circuit photocurrent density (mA cm^{-2}), and φ is the incident radiative flux (mW cm^{-2}). Photovoltaic performance was measured by using a metal mask with an aperture area of 0.09 cm^2.

Absorption measurements were preformed using Jasco V-670 spctrophotometer.

Profiler. The thickness measurements of the TiO_2 films were performed by Veeco Dektak 150 profiler.

Extra High-Resolution Scanning Electron Microscopy (XHR-SEM). The images were obtained by using Magellan XHR SEM of FEI (Field Emission Instruments), The Netherlands. The measurement conditions were 5 kV at various magnifications, as seen on the data bar of the images.

Ultrahigh-Resolution Scanning Electron Microscopy (UHR-SEM). The images were obtained by using Sirion UHR SEM of FEI (Field Emission Instruments), The Netherlands. The measurement conditions were 5 kV at various magnifications, as seen on the data bar of the images.

ASSOCIATED CONTENT

Ⓢ Supporting Information

Experimental section, table of PV results of the different concentrations using the spin deposition technique, J−V curves of the samples made by the spin deposition technique, and Tauc plots for the different hybrids samples. This material is available free of charge via the Internet at http://pubs.acs.org.

AUTHOR INFORMATION

Corresponding Author
*E-mail: lioz.etgar@mail.huji.ac.il.

Notes
The authors declare no competing financial interest.

■ REFERENCES

(1) Kojima, A.; Masashi, I.; Kenjiro, T.; Tsutomu, M. Highly Luminescent Lead Bromide Perovskite Nanoparticles Synthesized With Porous Alumina Media. *Chem. Lett.* **2012**, *41*, 397−399.

(2) Kagan, C. R.; Mitzi, D. B.; Dimitrakopoulos, C. D. Organic-Inorganic Hybrid Materials as Semiconducting Channels In Thin-Film Field-Effect Transistors. *Science* **1999**, *286*, 945−947.

(3) Mitzi, D. B.; Field, C. A.; Schlesinger, Z.; Laibowitz, R. B. Transport Optical and Magnetic Properties Of the Conducting Halide Perovskite $CH_3NH_3SnI_3$. *J. Solid State Chem.* **1995**, *114*, 159−163.

(4) Burschka, J.; Pellet, N.; Moon, S. J.; Humphry-Baker, R.; Gao, P.; Nazeeruddin, M. K.; Grätzel, M. Sequential Deposition As A Route To High-Performance Perovskite-Sensitized Solar Cells. *Nature* **2013**, *499*, 316−319.

(5) Liu, M.; Johnston, M. B.; Snaith, J. H. Efficient Planar Heterojunction Perovskite Solar Cells by Vapour Deposition. *Nature* **2013**, *501*, 395−398.

(6) Wang, J. T.W.; Ball, J. M.; Barea, E. M.; Abate, A.; Webber, J. A. A.; Huang, J.; Saliba, M.; Sero, I. M.; Bisquert, J.; Snaith, H. J.; et al. Low-Temperature Processed Electron Collection Layers Of Graphene/TiO_2 Nanocomposites In Thin Film Perovskite Solar Cells. *Nano Lett.* **2014**, *14*, 724−730.

(7) Stranks, S. D.; Eperon, G. E.; Grancini, G.; Menelaou, C.; Alcocer, M. J. P.; Leijtens, T.; Herz, L. M.; Petrozza, A.; Snaith, H. J. Electron-Hole Diffusion Lengths Exceeding 1 Micrometer In An Organometal Trihalide Perovskite Absorber. *Science* **2013**, *342*, 341−344.

(8) Xing, G.; Mathews, N.; Sun, S.; Lim, S. S.; Lam, Y. M.; Grätzel, M.; Mhaisalkar, S.; Sum, T. C. Long-Range Balanced Electron- And Hole-Transport Lengths In Organic-Inorganic $CH_3NH_3PbI_3$. *Science* **2013**, *342*, 344−347.

(9) Etgar, L.; Gao, P.; Xue, Z.; Peng, Q.; Chandiran, A. K.; Liu, B.; Nazeeruddin, Md.K.; Grätzel, M. Mesoscopic $CH_3NH_3PbI_3$/TiO_2 Heterojunction Solar Cells. *J. Am. Chem. Soc.* **2012**, *134*, 17396−17399.

(10) Laben, W. A.; Etgar, L. Depleted Hole Conductor-Free Lead Halide Iodide Heterojunction Solar Cell. *Energy Environ. Sci.* **2013**, DOI: 10.1039/C3EE42282H.

(11) Shi, J.; Dong, J.; Lv, S.; Xu, Y.; Zhu, L.; Xiao, J.; Xu, X.; Wu, H.; Li, D.; Luo, Y.; et al. *Appl. Phys. Lett.* **2014**, *104*, 063901−4.

(12) Aharon, S.; Gamliel, S.; Cohen, B. E.; Etgar, L. Depletion Region Effect of Highly Efficient Hole Conductor Free $CH_3NH_3PbI_3$ Perovskite Solar Cells. *Phys. Chem. Chem. Phys.* **2014**, DOI: 10.1039/C4CP00460D.

(13) Mosconi, E.; Amat, A.; Nazeeruddin, M. K.; Grätzel, M.; Angelis, F. D. First-Principles Modeling Of Mixed Halide Organometal Perovskites For Photovoltaic Applications. *J. Phys. Chem. C* **2013**, *117*, 13902−13913.

(14) Cai, B.; Xing, Y.; Yang, Z.; Zhang, W. H.; Qiu, J. High Performance Hybrid Solar Cells Sensitized by Organo Lead Halide Perovskites. *Energy Environ. Sci.* **2013**, *6*, 1480−1485.

(15) Edri, E.; Kirmayer, S.; Cahen, D.; Hodes, G. High Open-Circuit Voltage Solar Cells Based On Organic−Inorganic Lead Bromide Perovskite. *J. Phys. Chem. Lett.* **2013**, *4*, 897−902.

(16) Noh, J. H.; HyukIm, S.; Heo, J. H.; Mandal, T. N.; Seok, S. I. Chemical Management For Colorful Efficient And Stable Inorganic-Organic Hybrid Nanostructured Solar Cells. *Nano Lett.* **2013**, *13*, 1764−1769.

(17) Abrusci, A.; Stranks, S. D.; Docampo, P.; Yip, H.-L.; Jen, A. K.Y.; Snaith, H. J. High-Performance Perovskite−Polymer Hybrid Solar Cells Via Electronic Coupling With Fullerene Monolayers. *Nano Lett.* **2013**, *13*, 3124−3128.

(18) Kitazawa, N. Excitons In Two-Dimensional Layered Perovskite Compounds: $(C_6H_5C_2H_4NH_3)_2Pb(Br,I)_4$ and $(C_6H_5C_2H_4NH_3)_2Pb-(Cl,Br)_4$. *Mater. Sci. Eng.* **1997**, *B49*, 233−238.

(19) Ishihara, T.; Takahashi, J.; Goto, T. Optical Properties Due To Electronic Transitions In Two-Dimensional Semiconductors $(C_nH_{2n+1}NH_3)PbI_4$. *Phys. Rev. B* **1990**, *42*, 11099.

(20) Ishihara, T. Optical Properties Of PbI-Based Perovskite Structures. *J. Lumin.* **1994**, *60−61*, 269−274.

(21) HyoekIm, J.; Chung, J.; Kim, S. J.; Park, N. G. Synthesis, Structure, and Photovoltaic Property Of A Nanocrystalline 2H Perovskite-Type Novel Sensitizer $(CH_3CH_2NH_3)PbI_3$. *Nanoscale Res. Lett.* **2012**, *7*, 353−360.

17165

dx.doi.org/10.1021/jp5023407 | *J. Phys. Chem. C* 2014, 118, 17160−17165